Title

Canopy and Terrain Interactions Affecting Snowpack Spatial Patterns in the Sierra Nevada of California

Journal

Water Resources Research, 55(11)

ISSN

0043-1397

Authors

Zheng, Z
Ma, Q
Jin, S
et al.

Publication Date

2019-11-01

DOI

10.1029/2018WR023758

Peer reviewed

https://doi.org/10.1029/2018WR023758

Canopy and terrain interactions affecting snowpack spatial patterns in the Sierra Nevada of California

ZESHI ZHENG[1,*], QIN MA[2], SHICHAO JIN[3,4], YANJUN SU[2,3], QINGHUA GUO[2,3], AND ROGER C. BALES[1,2]

[1] *Department of Civil and Environmental Engineering, University of California, Berkeley, California, USA*
[2] *Sierra Nevada Research Institute, University of California, Merced, California, USA*
[3] *Institute of Botany, Chinese Academy of Sciences, Beijing, China*
[4] *University of Chinese Academy of Sciences, Beijing, China*
[*] *Corresponding author: zeshi.z@berkeley.edu*

Compiled October 27, 2019

Airborne light detection and ranging (lidar) is an emerging measurement tool for snowpack estimation, and data are now emerging to better assess multi-scale snow-depth patterns. We used airborne light detection and ranging (lidar) measurements from four sites in the southern Sierra Nevada to determine how snow depth varies with canopy structure and the interactions between canopies and terrain. We processed the point clouds into snow-depth rasters at 0.5×0.5-m^2 resolution, and performed statistical analysis on the processed snow-depth data, terrain attributes, and vegetation attributes, including the individual tree-bole locations, canopy-crown area, and canopy height. We studied the snow depth at such a fine scale due in part to the spatial heterogeneity introduced by canopy interception and enhanced melting caused by tree trunks in forested areas. We found that the dominant direction of a tree well, the area around the tree bole that has shallower snowpack, is correlated with the local aspect of the terrain; and the gradient of the snow surface in a tree well is correlated with the tree's crown area. The regression-tree based XGBoost model was fitted with the topographic variables, and canopy variables; and about 71% of snow-depth variability can be explained by the model.

http://dx.doi.org/10.1029/2018WR023758

Key Points:

- Lidar point density affects snow-depth estimates in dense forest with a warmer snowpack, over runoff-producing elevations in the Sierra.
- Under canopy, the deepest snow is generaly downslope from the tree bole.
- Across the rain-snow transition, peak snow accumulation was consistently greater in the open than under canopy.

1. INTRODUCTION

The snowpack in California's Sierra Nevada has long served as the primary water resource for agriculture and urban uses [1]. Spring snowpack measurements across mountain basins are the foundation of forecasts of water availability. As forecasts for both seasonal water supply and flood peaks following the onset of melt turn from statistical to spatial water-balance approaches, predictions require accurate estimates of both precipitation and snowpack water storage [2]. Quantifying the spatial distribution of snowpack properties in forested mountainous areas is a long-standing challenge in snow hydrology [3, 4]. In the high Sierra, orographic effects drive solid-phase precipitation falling over mid-to-high elevation regions. These areas are covered with heterogeneous densities of forest and a variety of vegetation [5, 6]. The mountain range's local topography introduces heterogeneity into the snow-surface energy balance, which further increases spatial variability in snow melt and total snow volume at different scales [7, 8]. Various vegetation types and canopy densities above the snow surface make answering this question even more challenging [9].

An important effect that coniferous canopies have on snowpack is the formation of tree wells, which are the areas with relatively lower snow depth under the canopy. Tree wells form during both snow accumulation and melting, dominantly by canopy interception, sublimation, and melt associated with enhanced incident thermal radiation to the snowpack, and unloading resulting in less accumulation of snow beneath canopies [10–13]. Other than snowpack quantity, these physical effects can also result in heterogeneity in snow density, grain size, and snowpack metamorphism [9, 10]. Understanding and being able

to quantify these effects can be beneficial as snow models are refined to better describe spatial heterogeneity. Prior studies in the southern Sierra Nevada using both ground measurements and lidar have reported about 40 cm less snow under canopy versus in the open during the main accumulation period, where mean snow depth in the open averaged about 1 m [14–16]. However, developing a predictive ability for the effect of canopy on snow accumulation and melt requires a more in-depth analysis of the influence [16].

Previous studies have discussed the topography-snow depth and vegetation-snow depth relationships either independently or mutually [17–19]. Regression and ensemble models were built for quantitatively analyzing each variable's impact on spatial patterns of snow depth [10, 20, 21]. Topographic variables such as elevation and northness are important in quantifying snow-depth spatial distribution, as orographic effects drive more precipitation at higher elevations and more energy on south-facing slopes drives snow to melt faster [14]. Leaf-area index (LAI) and distance from tree bole are two influential vegetation variables in determining snow-depth spatial distribution under canopies, the snow-depth variabilities caused by which are mostly due to varied capacities in intercepting snowfall; i.e., forest with higher LAI intercepts more snowfall and canopy leaves are less dense at the drip-edge than those are closer to the tree bole [22, 23].

However, observations regarding how topography and vegetation interactively affect snow depth have not been completely explored due to the lack of high quality field data in mountains [7, 24, 25]. Several control groups with respect to topographic variables and vegetation variables have to be sampled such that the altered effects across groups can be observed. Therefore, the number of samples needed will be a few times greater than in previous work. Also, varied topographic and vegetation conditions are preferred in study areas so as to extend the applicability of the results.

Regarding measurement techniques, canopy metrics like LAI can be retrieved from satellite imagery [26, 27], however, when studying on a finer resolution (meter or sub-meter), most previous studies were based on manual surveys [10, 20, 28], the samples of which are insufficient for drawing statistically significant conclusions. Techniques such as terrestrial laser scanning and unmanned aerial vehicles are emerging for forestry and agricultural studies [29, 30], and these techniques provide more samples comparing to manual surveys; however they have been used for extracting canopy metrics in snow hydrology studies in only a few cases [22]. Similar situations exist in snow-depth surveys using sensors, although ultrasonic snow-depth sensors can be used to continuously measure snow depth, the spatial densities of sensors are minimal comparing to the scale of mountains. Over the past two decades, with airborne lidar is also becoming more widely used in forestry and water resources mapping [31], as canopy structures can be detected and extracted using point-cloud data and image-processing algorithms [32–34]. In addition, by using change-detection techniques, spatial snow-depth mapping can be retrieved from snow-on and snow-off lidar scans over the same region [2]. With dense and widespread spatial measurements, it is expected that using lidar and aforementioned technologies can further narrow the knowledge gap of how terrain and canopy interactions affect the spatial distribution of snow.

The overall aim of the work reported here is to improve our understanding of canopy-terrain interactions on spatial patterns of snow depth in mountain forests. Using lidar data from four forested headwater areas in the southern Sierra Nevada, we addressed four questions. First, to what extent can one measure snowpack under canopy using airborne lidar of different measurement densities? Second, how do topography and canopy interactively affect local tree scale snow depth and tree-well patterns in forests of different tree densities. Third, how important are these effects for estimating basin-scale spatial snow quantities at different lidar measurement resolutions? Finally, how do differences in forest density affect snow-accumulation and melt patterns as measured by lidar?

2. DATA AND METHODS

We analyzed four lidar footprints collected in the southern Sierra Nevada, California (Figure 1). The lidar data were processed into point clouds, with point densities from 0.1 pts $\cdot$ m^{-2} to 10 pts $\cdot$ m^{-2} and raster data sets at resolutions from 0.5$\times$0.5 m^2 to 30$\times$30 m^2. The canopy-height models processed from the lidar footprints were processed with tree-segmentation algorithms. The snow depth and tree-well pattern beneath the segmented trees were evaluated relative to local topographic conditions and the samples analyzed to determine how terrain and vegetation affect the spatial snow-depth distribution. We also applied a machine-learning model to predict snow depth at 0.5-m resolution, with topographic and canopy related predictors, aiming for modeling the spatial distribution of snow depth at lidar resolutions.

A. Study areas and lidar data acquisition

The study areas, Bull Creek, Shorthair Creek, Providence Creek and Wolverton Basin, are headwater study areas of the Southern Sierra Critical Zone Observatory (SSCZO), three of which are located in the upper Kings River basin, with Wolverton 80 km south in the adjacent Kaweah River basin (Figure 1). The four study areas range from 1500 to 3500 m in elevation (Table 1). Vegetation density among all sites generally decreases in high-elevation subalpine forest, with Wolverton having a large area above treeline [35, 36]. The total surveyed area for both snow-on and snow-off data is about 150 km^2, with snow-on footprints collected in late March 2010, near peak accumulation, and snow-off footprints collected in August 2010. The 2010 water year had a wet snow season with mean snow depth of 2 m over the four sites [14]. The survey was performed by the National Center for Airborne Laser Mapping (NCALM) using Optech GEMINI Airborne Laser Terrain Mapper. The snow-on lidar data set has an average point density of 9.2 pts $\cdot$ m^{-2}, with the snow-off data averaging at 11.7 pts $\cdot$ m^{-2}. The data can be accessed from National Science Foundation's Opentopography web portal (Opentopography.org).

Our analysis was constrained by the availability of high-point-density lidar data. While there are other snow-on lidar data in the Sierra Nevada (e.g. NASA's Airborne Snow Observatory), their point density is too low for the under-canopy analysis we did here. We have smaller lidar data sets from other areas and dates, but they are much more restricted in elevation and canopy variables, limiting our ability for the space-time substitution in this 2010 data set [37].

B. Lidar data processing

The lidar data were processed to generate raster data. The raw point-cloud files were divided into 250 $\times$ 250-m^2 tiles using the LAStools software [38]. The accuracy of the lidar point cloud was compared with the snow-depth measurements from the wireless-sensor networks [39]. We extracted the ground

Table 1. Study sites general information

		Elevation range, m		Number of segmented	Slope, deg		Aspect, deg	
Site	Area, km^2	min	max	study plots (Section D)	min	max	min	max
Bull	20.7	1823	2490	37	9.5	22.3	114	264
Shorthair	5.4	2449	2753	6	12.4	16.7	81	219
Providence	18.4	1352	2218	32	10.7	27.0	145	258
Wolverton	48.0	1718	3496	84	12.8	64.7	21.3	306

points from each tile and interpolated them into a 0.5×0.5-m^2 resolution digital elevation model (DEM) using a simple kriging model with a spherical covariance function, using the ArcMap for Desktop and its ArcPy Python application programming interface [40]. The interpolated DEMs derived from both snow-on and snow-off lidar point clouds are accurate because of high density of ground-surface points. The average ground-surface point density for under-canopy points is higher than 4 pts $\cdot$ m^{-2} while the ground-surface point density for open area is higher than 8 pts $\cdot$ m^{-2}. According to [41], as the ground-surface point density is larger than 1 pt $\cdot$ m^{-2}, the root-mean squared error of the interpolated elevation estimate is less than 0.15 m, suggesting an accuracy validation of our interpolated snow-depth map for both under-canopy and open areas. We validated the under-canopy interpolation by using a cross-validation approach, in which we extracted ground lidar points under each segmented tree, trained a simple kriging model with a spherical covariance function using 80% of the ground points, and then evaluated the kriging model on the remaining 20% of the ground points. The root-mean squared error over 1564 segmented trees and 133687 ground points is 0.13 m, which is less than the 0.15 m reference given in [41], indicating that the interpolated DEM is accurate for both open and under-canopy areas. The 250×250-m^2 DEM tiles were mosaicked to form a single DEM for each individual study area.

A digital surface model (DSM) was generated from all first returns of the lidar point cloud. We produced a canopy-height model (CHM) by subtracting the DEM from the DSM. By using the watershed-segmentation algorithm [42], individual trees can be segmented from the canopy-height model. The snow-depth pixels beneath each tree were also extracted.

C. Lidar point-density analysis

The lidar point density (ρ) was calculated by dividing the total number of points by the projected concave area on the two-dimensional (2-D) xy-plane. On average, about 5% of the point cloud are ground points over a forested area [43] (we have tested our data set and the percentage was much greater than 5%), suggesting that at least 40 ground points can be measured under a tree with a crown diameter of 10 m when the point density is about 10 pts $\cdot$ m^{-2} and thus the snow-surface profile should be observable. However, how the low point density influences the total snow volume (snow depth multiplied by area) or snow water equivalent (SWE) is still unclear [14]. In order to study the changes of lidar-derived total snow volume with the lidar point density, this study randomly resampled the snow-on point cloud data with a density ρ at a variable percentage (ρ'/ρ, $\rho' \leq \rho$) to get points with different densities (ρ'). Each dataset with various point densities was used to interpolate a snow-depth product using kriging, as noted above. The total volume of snowpack derived from each data set with resampled point-cloud density was calculated for comparison. We also explored how various DEM resolutions (from 0.5 m to 30 m) influence the estimated snowpack volume. The DEMs with various resolutions were generated from the original point cloud.

D. Study-plot segmentation

The terrain of the four study areas were lumped into one data set for analysis, giving a broad elevation range, mild and steep slopes, and various aspects. Exploring interactions between terrain and vegetation over areas with heterogeneous topography is a non-trivial task because of the confounding effects from multiple topographic attributes. One solution is to control the potential confounders by making their values in a narrow range. Thus, we segmented each study area by using the National Agriculture Imagery Program (NAIP) dataset, topographic data layers, and Felzenszwalb segmentation algorithm [44]. The algorithm merges pixels based on neighboring pixels' similarities, and by doing so the neighboring pixels with similar topography and vegetation densities can be merged and thus the value ranges of confounders can be controlled in a narrow range within a single segment. We used the algorithm implemented in the scikit-image [45] Python library for segmenting the multi-channel imageries. On average, the size of the segmented study plots is 0.4 km^2.

E. Statistical analysis and modeling

E.1. Terrain and canopy attributes from lidar

The spatial distribution of snow in mountainous forested areas is controlled by orographic effects, wind redistribution, and canopy [5, 6, 46]. Other than canopy, the rest of the spatial variability of snow depth is largely related to the topography of the area. The snow-depth dependency can be represented by the following equation

$$h = f(t, c) \quad \textbf{(1)}$$

where h stands for snow depth, t stands for topographic variables, and c stands for canopy variables. In our study, the topographic variables are elevation, slope, aspect, northness, and topographic ruggedness index [47]. The canopy variables are canopy height, and distance to tree bole. To study the snow-depth profiles of tree wells, both globally and under certain terrain circumstances, we extracted the distance to tree bole and direction from tree bole of each individual snow-depth pixel, using the coordinates of the pixel and the segmented tree polygon.

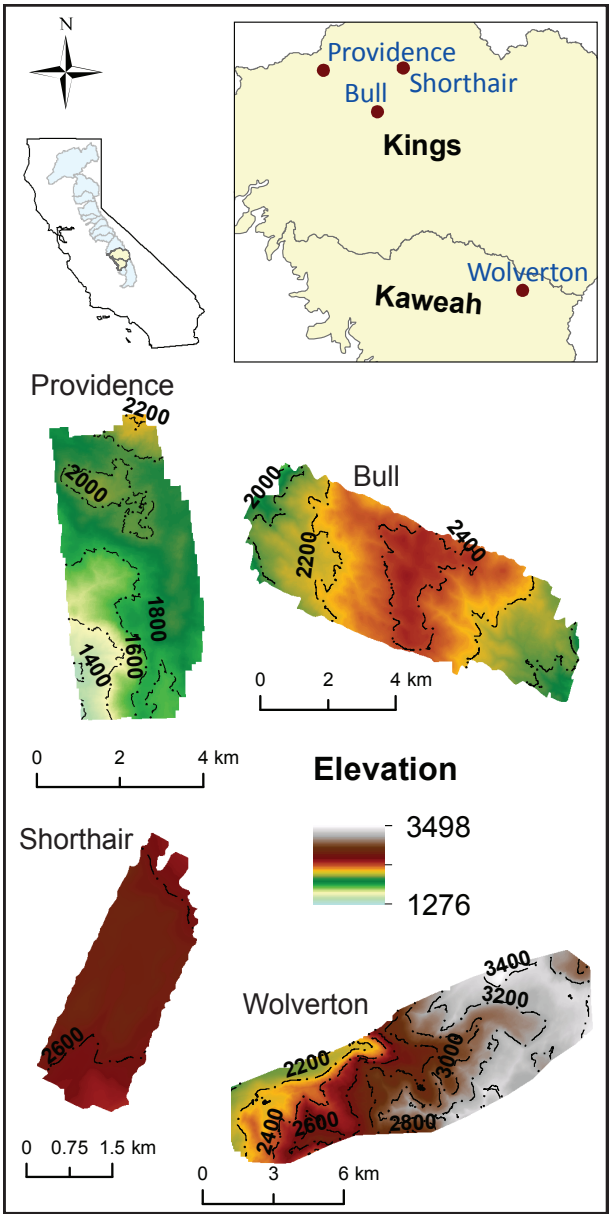

Fig. 1. (a) The study areas are located in two watersheds: Kings river, and Kaweah river basins of the Sierra Nevada mountains. Providence, Shorthair, and Bull are in the upper Kings river, whereas Wolverton is on the boundary of Kings river and Kaweah river basins. (b) Digital elevation model derived from lidar footprints of the six study areas.

We used the centroid of each segmented tree polygon as the tree bole location. The distance was calculated as

$$r = \Delta x^2 + \Delta y^2 \tag{2}$$

whereas the direction was calculated as

$$\theta = \arctan(\frac{\Delta y}{\Delta x}) \tag{3}$$

where Δx and Δy are distances the tree bole in x and y directions, respectively. θ was further converted from $[-180°, 180°)$ to $[0°, 360°)$ so θ is consistent with the aspect of the terrain. For each snow-depth pixel under the canopy, we calculated the standard deviation of the height of the tree above, and its crown area. In addition, we extracted a 5-m-radius circular area surrounding each snow-depth pixel and calculated the percentage of canopy-height pixels that are above 2 m. The 2-m threshold was chosen for eliminating the under-canopy vegetation from the calculation [14]. Outside the 5-m radius the canopy coverage was less correlated with snow depth.

E.2. Terrain and canopy interaction

We sampled study plots from the segmentations described in Section D. As the aspect of certain study plots can be highly variable, we filtered the segmentations whose standard deviations of aspects were larger than 50°. For the remaining sampled plots, we developed two approaches to analyze the terrain-canopy interactions relative to snow depth.

For the first approach, we divided the plots into four groups by north, east, south, and west aspect based on the mean aspect value of each plot. The north group has plots with mean aspect in the range of $0°-45°$ and $315°-360°$. The east group has plots in the range of $45°-135°$. The plots in the south and west groups have 90° and 180° increments, respectively, based on the range of the east group. We then randomly sampled 10 plots from each group with replacements, meaning that we allow repeating samples in the sampled 10 plots. The reason for using replacements is because there were only 9 plots available in the west group. We verified that the samples from the north, east, and south groups were representative with regards to the distributions of topographic variables (Figure 2). The west group only covers a narrow range of elevation, which can be a biased sampling group for this analysis. For each sampled plot, we binned θ at a 30° increment. The snow-depth pixels were aggregated and the mean of snow depth was calculated for each bin of θ. Then the mean snow depths were visualized versus θ over the polar coordinate system for each group separately.

For the second approach, all remaining segmented plots from the filtering noted above were analyzed individually. Here we define the center of mass of all normalized snow-depth-pixel values under canopies.

$$\Delta x_c = \frac{\sum_{i=1}^{n} \Delta x_i \times h_i}{\sum_{i=1}^{n} h_i} \tag{4}$$

$$\Delta y_c = \frac{\sum_{i=1}^{n} \Delta y_i \times h_i}{\sum_{i=1}^{n} h_i} \tag{5}$$

The coordinates of the calculated center of masses can be converted to polar coordinates using Equation (2) and (3) to get the distance r_c and the direction θ_c from the tree bole to the center of mass. We conducted a regression analysis between θ_c and the local aspect direction, r_c and local slope steepness of each study plot.

Both independent and dependent variables in the regressions were derived from a series of processing steps over the study plots that have a mixture of terrain and canopy conditions. To make the regression analysis more robust, we detected outliers over the 4-D space $(\theta_c, r_c, \text{aspect}, \text{slope})$ using an elliptic envelope approach that was implemented in the scikit-learn Python library [48]. Here we assumed that the data over the 4-D space are normally distributed.

Other than the dominant directions of tree wells, the gradient of tree well, which describes the steepness of the snow surface from the tree bole to the drip edge, can be another index representing the spatial distribution of the tree-well snow depth. For

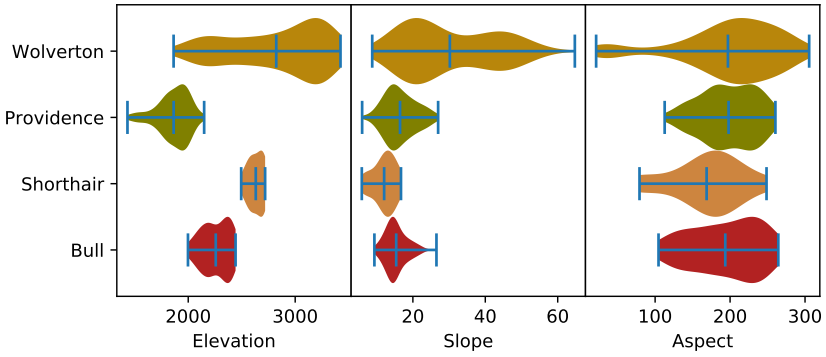

Fig. 2. The distribution of topographic attributes for all segmented study plots of each headwater catchment site.

each segmented tree, we extracted all snow-depth pixels under each tree and applied linear regression of snow-depth values versus their distance to the tree bole. The slope of the univariate regression was used to characterize the gradient of tree well. We investigated the relationship between the slopes of tree wells and crown area of trees by binning the crown area from 0 to 20 m^2 at a 2-m^2 increment and calculating the mean tree-well slope for each bin. The analysis was conducted independently for four non-overlapping elevation bins that were derived by dividing the entire elevation range into four equal sections.

To assist in interpreting our findings on tree-well gradients from the perspective of snow melt, we used a degree-day method with the daily temperature data from the meteorological stations at these sites, as the incoming longwave radiation that strongly drives snow melt at early season and degree day is a good indicator of the magnitude of snow melt [49]. We selected 13 March as the starting date for accumulating the degree day because that is when the most recent precipitation ends. By using the temperature data and an empirical lapse rate of $6\ ^{\circ}\mathrm{C} \cdot \mathrm{km}^{-1}$ [50], we also estimated cumulative degree-day time-series from 1 March to 31 March for four different elevations, namely 1750 m, 2250 m, 2750 m, and 3250 m. In addition, we retrieved the snow-pillow snow water equivalent measurements from Upper Providence (1950 m), Tamarack Summit (TMR, 2300 m), and West Woodchuck Meadow (WWC, 2700 m). Both TMR and WWC data were downloaded from the California Data Exchange Center. These two sites were selected because they are geographically closer to the study areas and their local elevations are within the elevation ranges of the study areas. We compared the estimated snow melt at the meteorological stations and the observed snow melt at these snow-pillow sites from 13 March to 23 March.

The zonal statistics (mean, standard deviation) of tree-well snow depth were also retrieved and we engineered three canopy statistics: canopy-height standard deviation, crown area, and percentage of canopy coverage within a 10-m radius. We increased the radius for calculating the canopy coverage to make sure that the tree above can be included in this coverage statistic. The zonal mean values of snow depth were detrended by topographic variables before they were further investigated. Principal component analysis (PCA) is commonly used for projecting a set of possibly linearly correlated variables into uncorrelated variables. We used a biplot of PCA for interpreting the correlations between zonal statistics of snow and canopy; we estimated the bivariate distribution of variable pairs by using a Gaussian kernel density estimation.

E.3. XGBoost modeling of snow depth

In order to study how much spatial variability of snow depth these topographic and canopy variables can explain, we modeled the function f in Equation (1) by using an Extreme Gradient Boosting (XGBoost) model [51]. The XGBoost model is an ensemble involving a series of regression trees trained in an additive manner. We applied the XGBoost model to, first, detrend the snow-depth dependencies on the topographic attributes, and then to model the detrended residuals using canopy attributes. Compared to other ensemble methods such as Random Forest [52] and Gradient Boosting Machine [53], the XGBoost model has more hyperparameters that need to be tuned. Important parameters that affect model performance include: number of estimators (n_estimators), maximum regression tree depth (max_depth), minimum number of samples in a child node (min_child_weight), minimum loss reduction threshold (γ), percentage of data samples (subsample), percentage of attribute samples (colsample_bytree), $L1$ or $L2$ regularization parameters (α), and learning rate (λ). We tuned these parameters one after another by using a five-fold cross-validation scheme with an exhaustive grid-search approach. We gained two sets of parameters, one set for topographic attributes only and the other set for canopy attributes only. As the XGBoost approach is computationally intensive, we sampled 200,000 pixels from all lidar data for tuning and building the model. And the dataset is splitted with 80% of data points for training and 20% of data points for testing. The mean-squared loss was used for training the model,

$$L = \sum_{i}^{n} (y_i - \hat{y}_i)^2 \tag{6}$$

We evaluated the trained models by using the coefficient of determination R^2,

$$R^2 = 1 - \frac{\sum_i^n (y_i - \bar{y})^2}{\sum_i^n (y_i - \hat{y}_i)^2} \tag{7}$$

where y_i is the ith observed snow depth, $\bar{y}$ is the mean of all observations, and $\hat{y}_i$ is the ith model estimate. All computations were implemented using the XGBoost library and its Scikit-Learn application programming interface in Python.

3. RESULTS

We observed snow depth under canopy with both lidar point-cloud and 0.5×0.5-m^2 resolution imagery. By extracting a cross-section of canopy points from snow-off lidar point-cloud data and ground-surface points from snow-on lidar point cloud, we observed the snowpack surface under both dense and sparse canopies (Figure 3a, b). The under-canopy snow surface has a concave shape, versus flat in the open. A similar pattern was observed with rasterized snow-depth data (Figure 3c).

A. Snow depth interpolation using lidar with various point-cloud density

Overall, the lidar-derived total snow volume showed a slight increase with point density below $1-2$ pt $\cdot$ m^{-2}, but exhibited no consistent pattern at higher densities (Figure 4). The decreasing trend at Wolverton (Figure 4 d) is different than the other three sites is because more than half of the area at Wolverton is above the treeline so the site will be less affected by the vegetation. The decrease in point density only accounts for 0.5% more total snow volume at 3 sites, but a 20% increase at the lower-elevation Providence site. Moreover, the change of point density can influence the estimated spatial distribution of snow depth, with the interpolated snow surface becoming smoother at lower point densities (not shown). Changing DEM resolution (0.5-30 m) had little influence on estimated snow volume (Figure S1).

B. Dominant tree-well directions

For the first approach introduced in Section E.2, analyzing plots by dominant aspect, we observed that under-canopy snow-depth patterns also depend on aspect. Snow is generally deeper if the direction from the tree bole to the snow-depth pixel location is the same as the local aspect (downslope), with the upslope direction usually having the shallowest snowpack (Figure 5). Both north-slope and east-slope groups strongly indicate this pattern, with the downslope side having about 40% more snow than upslope. The south-slope and the west-slope groups have a weaker pattern, with the deepest directions shifted to the southeast and southwest, respectively, and deeper side having 10-15% more snow than the shallower side.

For the second approach in Section E.2, we found that the direction from the tree bole to the center of mass (θ_c) for under-canopy snow at each individual study plot is positively correlated with the local aspect ($R^2 = 0.47$ and $p < 0.01$) (Figure 6). The distance (r_c) from the tree bole to the center of mass is negatively correlated with the local slope of the study area ($R^2 = 0.17$ and $p < 0.01$), provided the 4-D outlier detection described in Section E.2 is used before the regression analysis. The first finding is significant and consistent with what was found using the first approach. This second finding implies that the interactions between canopy and local aspect will decay as the local slope becomes larger. In order to quantify the observed trends numerically, we parameterized a new variable, canopy-terrain shadow (CTS),

$$CTS = (1 - \sin(\text{slope})) \times \cos(\theta - \text{aspect}) \quad \textbf{(8)}$$

which can be used in pixel-level modeling. The correlation analysis (data not shown) shows that the snow-depth residuals detrended from topographic variables increase as CTS becomes larger ($p < 0.01$).

C. Tree-well gradients and under-canopy snow depth

The gradients of tree wells are correlated with canopy size. As crown area increases, the tree-well slopes become steeper for elevation bands below 2950 m (Figure 7). On average, the snowpack is 2 cm deeper for every 1 m away from the tree bole when the crown area is more than 8 m^2. Additionally, the slopes of tree wells are also correlated with topographic variables. However, the terrain effects can be altered as the phase of precipitation changes from rain to snow, and as snow melts. At Providence, which lies in the lower elevation range, tree-well gradients are correlated with elevation (Table 2). For roughness and slope of the landscape, at Shorthair, these two variables are positively correlated with the tree-well gradient, while opposite trends are observed at Providence and Wolverton. The correlations with roughness and slope are not significant at Bull.

Table 2. Correlation coefficient (R) and p-values calculated between tree-well gradients and topographic variables.

	elevation		northness		roughness		slope	
Study area	R	p	R	p	R	p	R	p
Bull	0.03	0.10	0.10	0.00	-0.01	0.51	-0.02	0.16
Shorthair	-0.02	0.24	0.02	0.31	0.16	0.00	0.17	0.00
Providence	0.23	0.00	0.07	0.00	-0.08	0.00	-0.09	0.00
Wolverton	-0.02	0.18	-0.04	0.01	-0.07	0.00	-0.06	0.00

The biplot (Figure 8a) from PCA indicates that the zonal average of snow depth is negatively correlated with all canopy attributes. The scatter plots in Figure 8 suggest some important correlations. First, while a taller tree and larger tree-height standard deviation can be expected to intercept more precipitation, the data suggest that the marginal effect from canopy height is stronger when the height is lower than 5 m. Also, the effect from an individual tree saturates as the standard deviation of canopy height reaches 4 m (Figure 8b). On average, the snowpack beneath a tree with near-constant height can be at least 0.2 m deeper than that under a tree with varying height (Figure 8d). However, the tree-height standard deviation is strongly correlated with average tree height, such that the causal effect cannot be identified with the current data set. Second, the strong effect from the surrounding canopy suggests that under-canopy snow depth is affected by the surrounding canopy as well as the tree above (Figure 8c). When trees are clustered together, the snowpack tends to be shallower, which is consistent with the findings from raw lidar visualization (Figure 3). Third, canopy volume does not significantly affect the mean under-canopy snow depth, but notably affect the standard deviation of snow depth (Figure 8e).

D. Prediction of snow-depth patterns

We first modeled snow depth using topographic variables only, which include elevation, slope, aspect, northness, and roughness. The tuned hyperparameters are shown in Table 3. By just using topographic variables, the testing R^2 equals 0.69, which is much higher than the Random Forest based model using the same data set [14]. By excluding the measurement error of 15 cm from lidar [54] from the total error of 43 cm, the testing root-mean-squared error (RMSE) is 40 cm. The snow-depth values were detrended using the best XGBoost model with topographic variables and

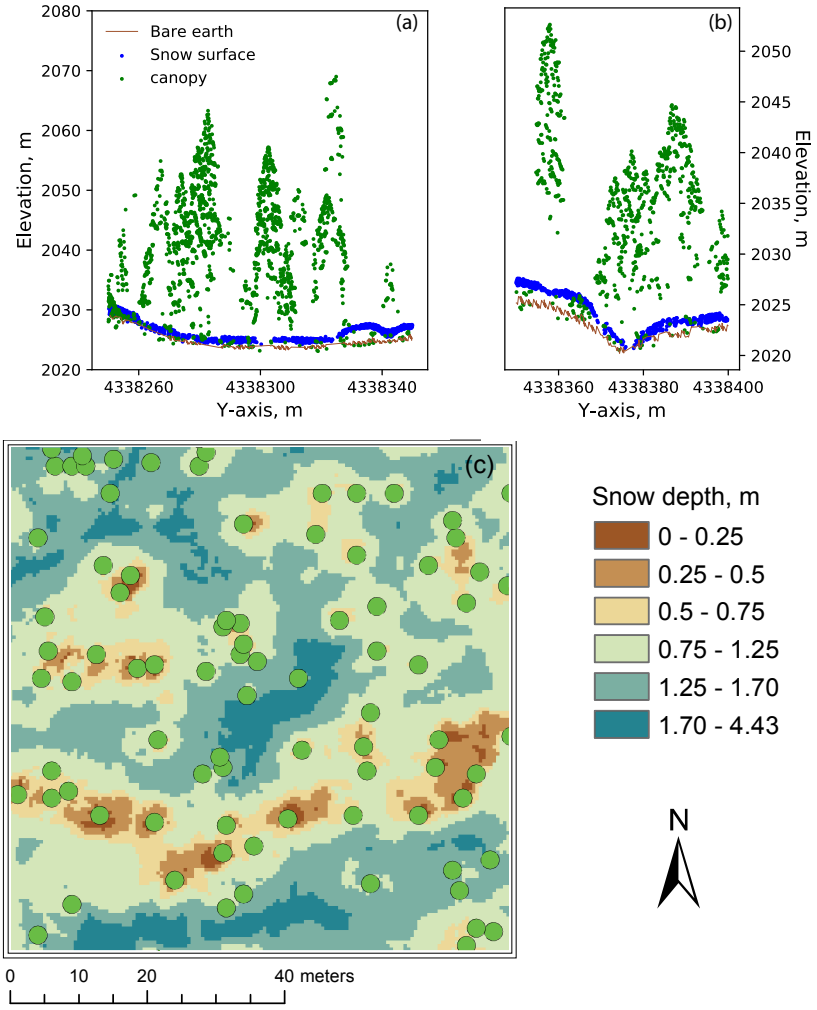

Fig. 3. Snow-depth visualization using (a) point-cloud data with clustered canopies (b) sparse canopies, and (c) rasterized snow-depth with green markers, which are the tree tops detected from the canopy-height model using the tree-segmentation algorithm.

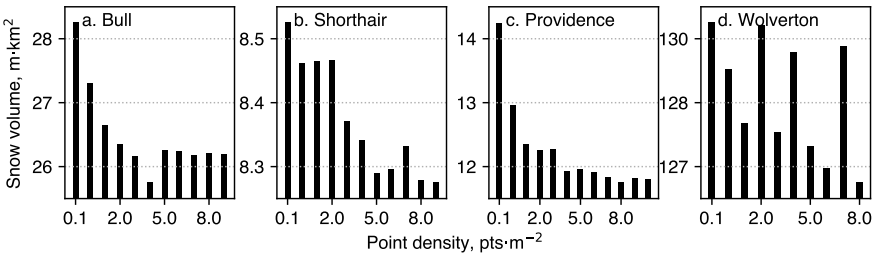

Fig. 4. Changes of lidar-derived total snow volume with the lidar point density at (a) SSCZO Bull site, (b) Shorthair site, (c) Providence site and (d) Wolverton site.

the detrended residuals were modeled with the canopy variables (canopy height, distance to tree bole, and canopy-terrain shadow). However, the spatial variability that can be explained from the canopy variables is almost negligible over an area with significant elevation differences, compared to that from topographic variables. The *CTS* variable is also the least important variable among the three. The first two regression-tree structures (Figure S2) show that, the canopy-terrain shadow started splitting data from the second regression tree, which confirmed it is weaker compared to the other canopy-related variables. Canopy variables become important after removing elevation. Across a wide elevation range, model combining topographic and canopy variables has a slight improvement, with testing RMSE = 39 cm and $R^2 = 0.71$. At Providence, we found that

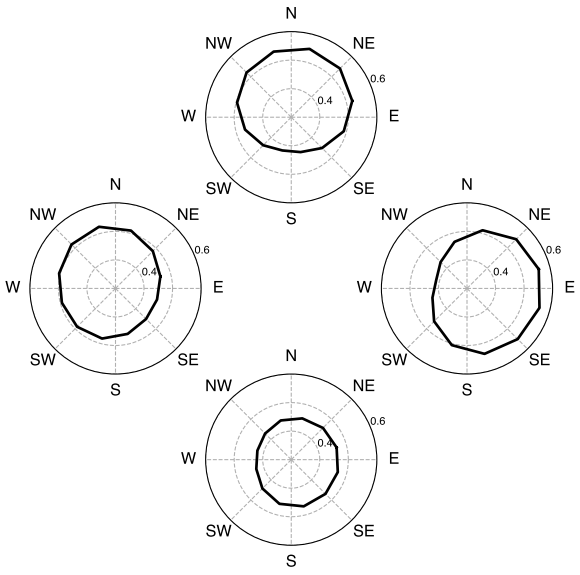

Fig. 5. Averaged normalized snow depth under individual segmented canopy over each direction bin at slopes with four different slope aspects: north, east, south, and west (clockwise from the subplot on the top). The snow depth is higher in the direction that is consistent with the local aspect, i.e., for a north facing slope, the snow under the north side of the canopy is deeper whereas under the south side is shallower.

the ratio of the snow depth in open area and under canopy did not change within the 1700-2100 m elevation range, where we had the majority of observations (Figure 9a-c).

Table 3. XGBoost model hyperparameters tuning results

		Tuned value		Tuned loss	
Parameters	Tuning range	Topo	Canopy	Topo	Canopy
n_estimators	0-5000	3000	3000	0.174	0.10486
max_depth	2-12	9	3	0.156	0.10404
min_child_weight	1-6	5	4	0.156	0.10404
γ	0.1-0.5	0.4	0.2	0.1559	0.10403
subsample	0.6-0.9	0.9	0.7	0.1554	0.10401
colsample_bytree	0.6-0.9	0.9	0.7	0.1554	0.10401
α	0-1	1e-5	1e-5	0.1554	0.10401
learning rate	0-1	0.01	0.01	0.1552	0.10401

4. DISCUSSION

A. Lidar point-cloud density effect on snow-depth estimation

The lidar point density had no significant influence on the estimation of total snow volume, although it can influence the mapped spatial distribution of snow depth. The main reason for this may be the overall smoothing effect of low-density lidar

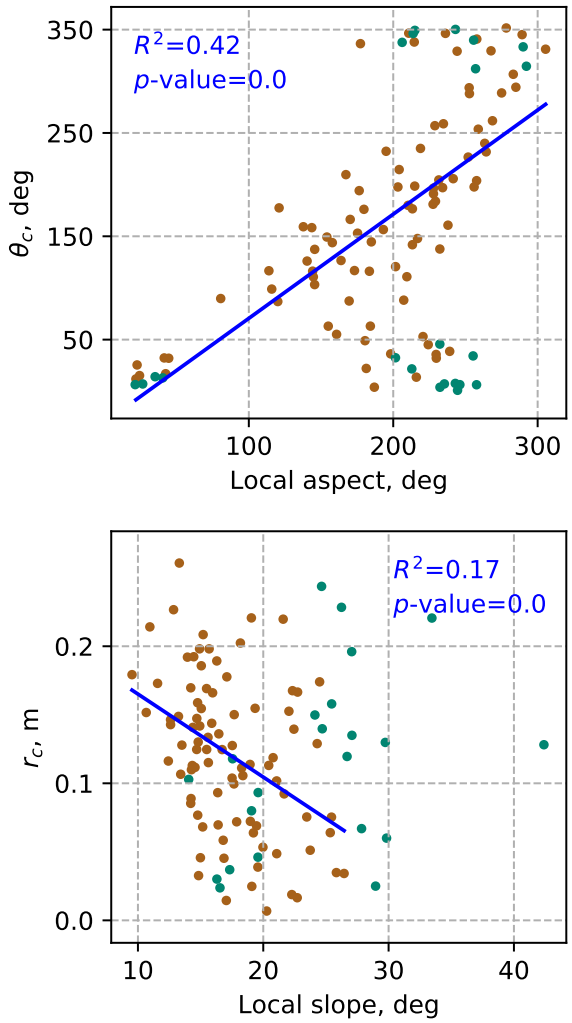

Fig. 6. (a) The direction from center of tree wells to the tree boles (θ_c) versus local aspect and (b) the distance from center of tree wells to the tree boles (r_c) versus local slope. The green markers are outliers detected from the multivariate outlier-detection algorithm.

data. The low point density may result in under-sampling of tree wells, which leads to an overestimation in the rasterized snow-depth products and total snow volume. However, the low point density may also result in under-sampling points in open and drip-edge areas with higher snow depth, which leads to an underestimation of total snow volume. The overestimation of snow depth in tree wells and the underestimation at snow peaks may balance the total snow volume estimation. However, with greater vegetation coverage, the overestimation in tree wells may become larger than the underestimation in the open. This might be the reason for the sharp increase of total snow volume at Providence when the point density becomes lower than 1 pt $\cdot$ m^{-2}. Providence has a relatively larger vegetation coverage than the other three sites. [41] suggested that a point density of 1 pt $\cdot$ m^{-2} is enough to generate DEM with very high accuracy, and the further increase of point density cannot bring significant change in the DEM accuracy. Therefore,

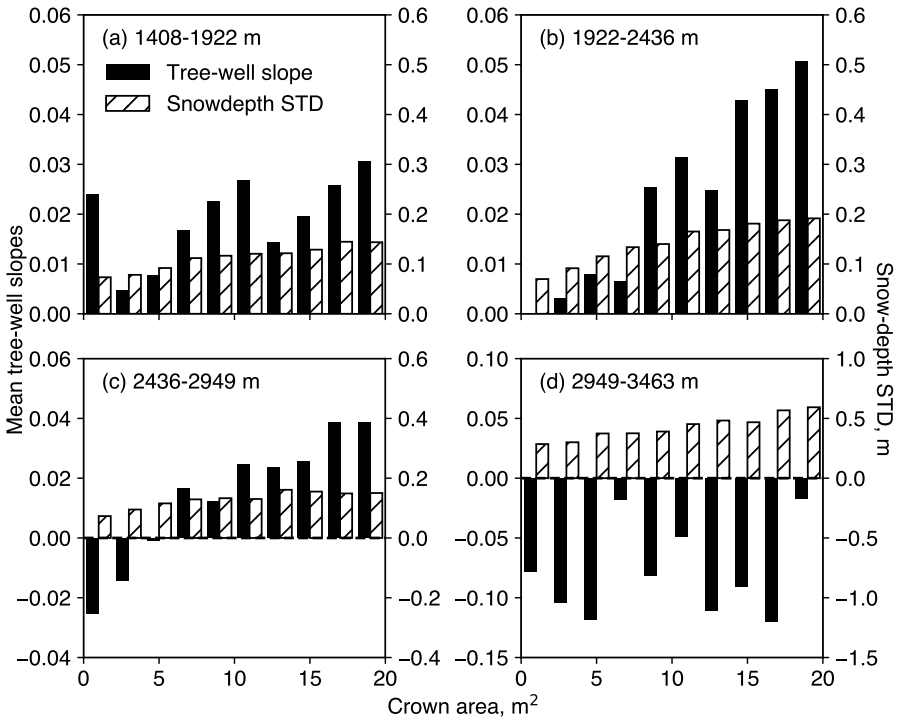

Fig. 7. Tree-well slopes and snow-depth standard deviations for all tree wells versus crown areas by four elevation bands, indicating that as the crown area growing larger the snow-depth will have a wider distribution, and the tree-well gradient will become steeper except at the highest elevations.

we suggested that a minimum of 1 pt $\cdot$ m^{-2} lidar point density should be achieved for snow-depth estimation for cases without rain and before melt, i.e. the 3 higher elevation sites shown in Figure 4. We calculated the average snow-surface point density for areas under canopy. The average point density is more than 4 pts $\cdot$ m^{-2} as the distance to tree-bole is less than 1 m and the density increases to more than 8 pts $\cdot$ m^{-2}. The point density we have under canopy is much higher than the 1 pt $\cdot$ m^{-2} threshold introduced in [41] and the interpolated under-canopy snow depth should be accurate enough for tree-well analysis.

The DEM resolution had no significant influence on the estimation of total snow volume, and the reason might be related to the estimation in the kriging algorithm. We are not elaborating on that as interpolation algorithms are not the focus of this study.

B. Snow-depth distribution within tree wells

The formation of tree wells is caused by canopy interception and faster snow ablation beneath the canopy, which is driven by heterogeneity in surface-energy inputs. In a forest, both canopy interception and the snow-depth distribution in tree wells observed from the lidar data can be due to non-symmetrical energy inputs from the atmosphere and forests, wind redistribution, and creeping of the snowpack. In forested snow-covered areas, longwave radiation varies the most at different canopy-cover conditions [13]. Consider the equation below,

$$L_{\downarrow} = v(\sigma_a \delta T_a^4) + (1 - v)(\sigma_c \delta T_c^4) \quad \textbf{(9)}$$

where σ_a and σ_c are the dimensionless effective emissivities for atmosphere and canopies; T_a and T_c are air temperature and canopy temperature; δ is the Stefan-Boltzmann constant (5.67×10^{-8}W $\cdot$ m^{-2} $\cdot$ K^{-1}); v is the canopy openness, usually represented by the sky-view factor (SVF) for a sub-canopy location [55]. The SVF in the upslope direction from the tree bole will be much smaller than in the downslope direction assuming the tree bole is upright. Despite that the emissivity of trees being higher than that of the atmosphere [56], the shortwave radiation absorbed by the canopy can heat up the tree leaves and tree boles [57, 58], which makes T_c higher than T_a. This explains that the shallowest snowpack can usually be observed around the tree bole because of the heat emitted. Also, more meltwater drip exists around the tree bole than the drip-edge because more snow was intercepted during snow accumulation around the tree bole area, which accelerate the snowmelt on the ground [59]. Thus from Equation 9, the total longwave radiation that enters the snow surface in the upslope direction under canopy will be higher, which is consistent with the observed centers of mass of tree wells being downslope (Figure 5, 6). Considering the steepness of slopes, the SVF in the downslope direction should increase as slope becomes steeper [60]. However, our observations are counter-intuitive, as the distance between the tree-well center of mass and tree bole (r_c) decreases as slope increases, which is likely due to inaccurate slope estimation because it was estimated by averaging slopes at finer resolution within the study plot. The correlation analysis (Figure S3) between the local slope at each canopy and r_c suggests that a steeper slope will result in more snow creep, which is a similar finding as was reported in [57]. We also retrieved the wind speed and wind direction data from the on-site meteorological stations. We inspected the wind-direction distribution prior to the date that the lidar were scanned, and since the last snowfall. But the wind

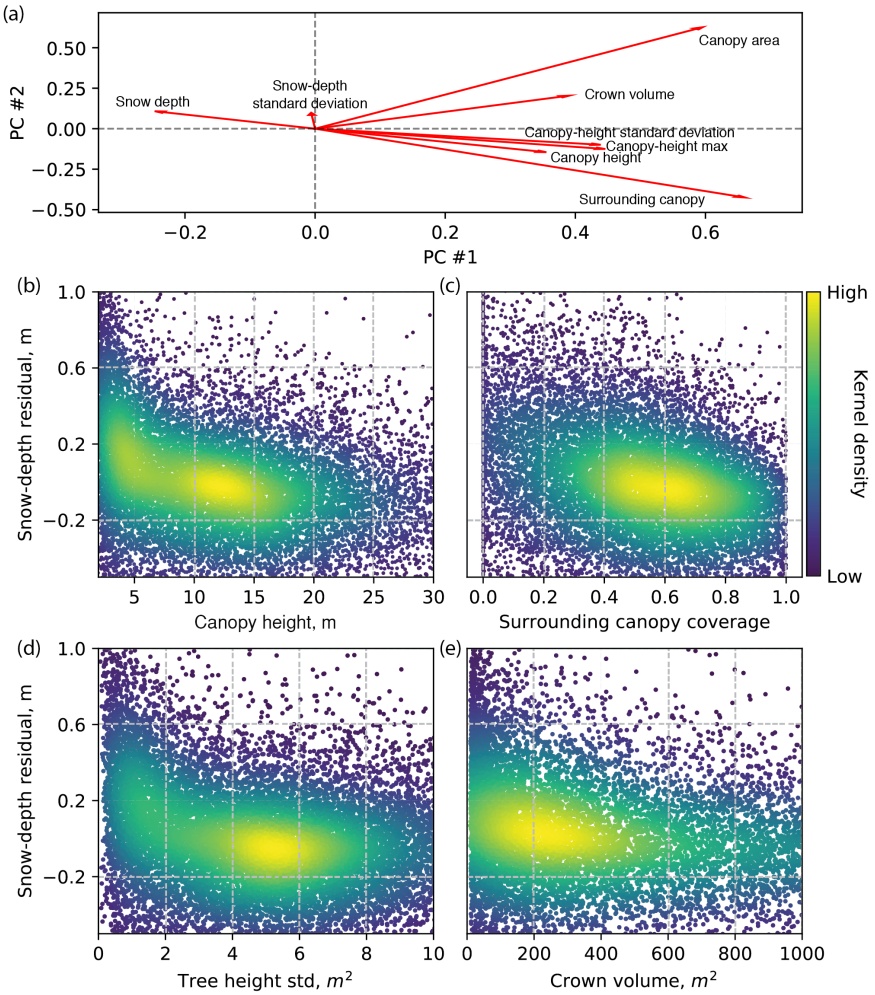

Fig. 8. (a) Principal component analysis bi-plot of 8 variables, including two snow related variables: snow depth, snow-depth standard deviation; and six canopy-related variables: canopy area, crown volume (total volume from tree crown base height to crown top), canopy height, canopy height max, canopy height standard deviation, and surrounding canopy coverage (percentage of canopy covered area within 10-m radius). Detrended under-canopy snow depth zonal mean versus four major canopy variations in (b) canopy height, (c)surrounding canopy coverage, (d) tree height standard deviation, (e) crown volume.

directions are random, which suggests the observed tree-well snow distribution was not affected by wind.

C. Canopy effects and canopy-terrain effects

The terrain slope affects the interactions between canopy and terrain on the snowpack. The outliers shown in Figure 6 indicated that the majority of outliers are on steeper slopes, which suggests that on steeper terrain, the terrain-canopy interactions will be less likely to explain any further snow-depth distribution of the tree well.

Intuitively, larger tree canopies seem to be able to make the tree wells larger and deeper. This can also be explained from the perspective of energy inputs. The tree height, crown area, and tree-bole diameters are highly correlated in common cases [61]. Therefore, the longwave radiation absorbed by the snow surface or emitted by the canopy and tree bole is usually higher when it is under a tree with larger crown area and at the same distance to the tree bole. From Figure 7a-c, we observed that both tree-well gradients and snow-depth standard deviation increase as the crown area increases. This can also be due to larger crown intercepting more snow during snowfall. As a result, the mean snow depths under larger canopies are usually shallower. However, Figure 7d shows the opposite trend compared to other elevations, with snow depth being negatively correlated with the distance to the tree bole. This suggests there is no snow melt yet at the elevation above 2950 m because the temperature was lower and the total energy inputs was not enough to drive snow melt. An alternative explanation, based on observation in Oregon Cascades, is that the orographic enhancement of precipiation is greater at high elevations, with canopy interception reaching a maximum holding capacity and thus more under-canopy snow [62].

While snow intercepted by canopy can increase sublimation, much of the intercepted snow in the Sierra Nevada can also undergo mass unloading and fall to the snowpack as snow or meltwater. Our data had insufficient resolution to probe this

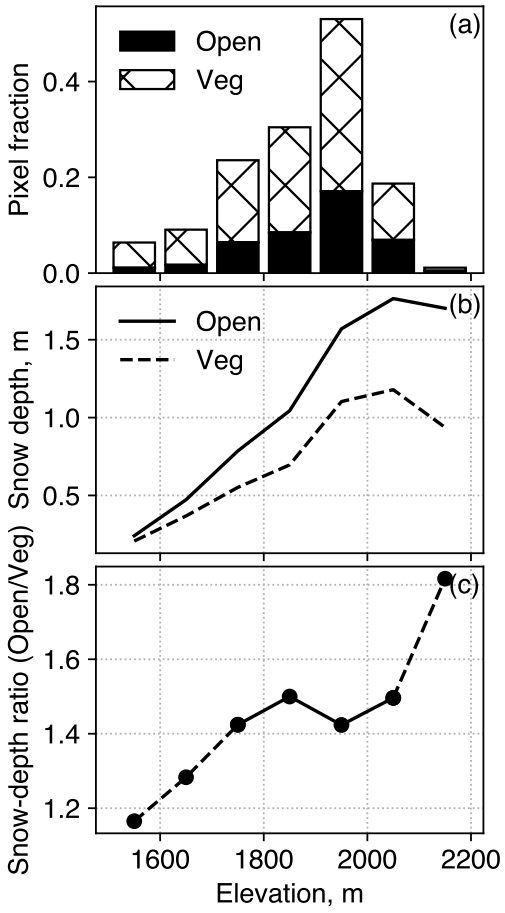

Fig. 9. (a) The pixel density histogram of the lidar data in open area and under canopy at Providence, (b) the mean snow depth in the open area and under canopy, and (c) the snow-depth ratio between in the open and under canopy along the elevation gradients at 100-m increment. The solid line represents the region where has 90% of the total vegetated area at Providence.

question, but future studies with repeat, ground-based lidar should could provide insight into this question.

The tree-well gradients are correlated with elevation (Table 2) at Providence but not in the other sites, which can be attributable to several reasons. First, the precipitation is more often mixed rain and snow at lower elevations, and warmer temperature accelerates snow melt both in the open and under canopy. This can make the tree-well gradients less steep compared to areas where precipitation is mostly snow. It can also be caused by the earlier snow melt at lower elevations. The mean snow depth along the elevation gradients at Providence (Figure 9b) suggests that melt rates were similar in the open area and under canopy at lower elevations, but started to differ as elevation increased. We should have observed similar snow-depth differences with elevation if the melt rates are similar. A confounding factor is that there were fewer observations at lower and higher versus mid elevations. The meteorological station at Upper Providence has the greatest degree-day value compared to others. Intuitively, the lower meteorological station at Providence should have a higher degree-day value, with the inconsistent pattern attributed to the differences in microclimate and energy exchange [63]. The cumulative degree-day time series estimated for four elevations (Figure 10) using an empirical lapse rate of 6 $^{\circ}C \cdot km^{-1}$ [50] and observed temperatures (Table 4), indicates that lower elevations had earlier snow melt and there was no snow melt above 3000 m before the lidar flight. The longwave energy gradient with elevation is driving the distribution of tree-well gradients, which matches the correlation between tree-well gradients and elevation at Providence (Table 2). The zero cumulative degree days at 3250 m helps explain the contrast in Figure 7d, as there was no snow melt and thus the under-canopy snowpack was randomly distributed. From the snow-pillow measurements (Table 4), we observed that the snow melt at Taramack Summit was less than 1/3 of that at Upper Providence and the snowpack at West Woodchuck Meadow did not melt at all, which supports the degree-day calculation.

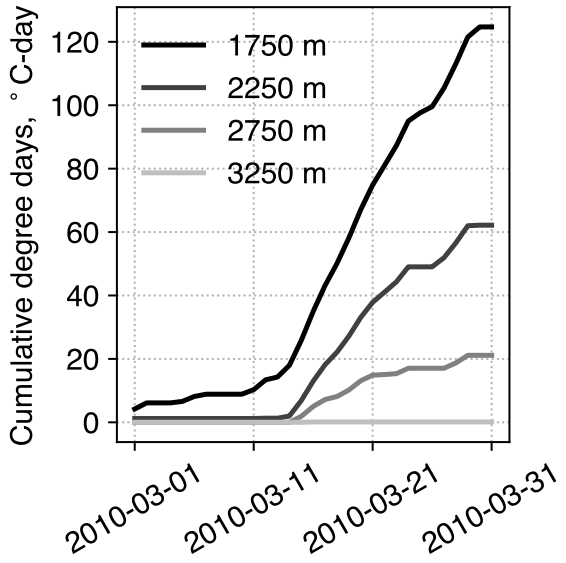

Fig. 10. Degree-day estimation using empirical lapse rate and temperature measurements for 4 elevations.

Table 4. Degree day and snow melt from 13 March to 23 March, 2010

	Lower Providence	Upper Providence	Lower Bull	Wolverton	TMR	Upper Bull	Panther	Shorthair	WWC
Degree day, °C	51.0	76.0	40.0	25.0	N/A	55.0	48.0	45.0	N/A
ΔSWE, cm	N/A	-9.6	N/A	N/A	-2.7	N/A	N/A	N/A	-0.3
Elevation, m	1753.0	1981.0	2195.0	2218.0	2300.0	2461.0	2618.0	2708.0	2773.0

The degree-day calculation also suggests that differences in under-canopy snow, and by extension the point density needed to characterize differences, are more important in denser forests under warmer conditions, i.e. lower elevations or later in the season at high elevations. Canopy effects observed from one-time lidar data are net effects, reflecting both canopy interception during accumulation and longwave radiation during melt. These effects becomes observable from lower elevation to high elevation as time elapses [16]. Our current observations from a

single lidar scan provide a window on these effects, knowledge of which can be refined by repeating the analysis with lidar scans a few weeks apart at the same location, in subsequent years, making lidar measurements in wet versus dry years at the same location, and sampling different locations to provide more-variable conditions than present in the current data.

We also experienced some difficulties in applying the newly parameterized variable, canopy-terrain shadow (*CTS*), in the XGBoost model. We compared the variable importance based on two metrics, number of regression tree nodes that use the variable to split, and the information gain from the variable. We observed that *CTS* has the 4th most node splits but has the least information gain, suggesting that for the current lidar data set, uncertainties in *CTS* increase when going to such a fine scale. Also, we were only able to observe the trends by averaging snow depth in different aspects (Figure 5) or using the center-of-mass of all normalized tree-well snow depth (Figure 6). But these trends are not usable for finer scale snow-depth modeling. A more-accurate canopy-segmentation algorithm and higher point-density lidar might be helpful in reducing the uncertainties in these canopy-related variables at finer resolution, and provide better modeling.

Another challenge related to the canopy effect is that some of the findings are based on the zonal statistics calculated from single trees. Although we observed these zonal statistics to be strongly related to the snow distribution under the canopy, it is challenging to transform them into usable variables that can be integrated into pixel-based models. Transfer functions or some new canopy-related features need to be developed to account for these influences. Further, extending the analysis with addtional high-density lidar data in the dense forests of the Sierra Nevada to evaluate effects of 2-4 weeks before and after peak accumulation, in both wet and dry years, could enhance the predictive ability for forest-canopy effects on the Sierra snowpack.

D. Implications for water resources management

Understanding how the snowpack interacts with canopy and terrain using actual dense measurements from lidar can improve spatially distributed hydrologic modeling that is based on mass balance of water across a watershed. Considering that Sierra Nevada watersheds, and others around the world rely on mountain snowpack as primary water supplies, streamflow predictions are heavily affected by the modeling of snow accumulation and melt. Thus, improving these interactions has great practical meaning in water resources management.

The trained regression model reached an R^2 of 0.71 at 0.5-m resolution. We can expect that resampling the 0.5-m results to a coarser resolution can make the R^2 even higher. Applying the trained model on the manipulated testing dataset at Providence, we found that a less-dense forest with only 10% the number of trees had a mean snow depth of about 1.2 m versus 1.0 m for the current forest. This is similar to the mean snow-depth ratio of 1.5 observed (Figure 9c). Taking into account the 2:1 ratio of open versus canopy-covered area suggests a 25% greater mean snow depth, which is similar to the 20% greater depth from the model simulation. Other than developing a deeper snowpack with less snow interception and slowing melt, managed reductions in forest density could also relieve water stress by reducing evapotranspiration [35].

The performance of the model implies that similar machine-learning methods can be practical for spatial prediction, or even spatio-temporal tasks when proper temporal features are available. On the other hand, training the machine-learning models is time-consuming and needs a great amount of training data. Gathering training data can be costly, so one may want to balance the cost and benefit before pursuing the statistical approach for estimating snow depth for practical purposes. Since we found that removing a large portion of lidar points does not affect the final estimates of total snow volume in areas that are not dense canopy, the detailed modeling at fine resolution may not be necessary for water management andthe coarser-scale lidar and satellite products being prpoposed for operational hydrology [64] may provide a sufficient guide.

5. CONCLUSIONS

The tree-well snow surface can be observed from airborne lidar with average ground-point density higher than 1 pt $\cdot$ m^{-2}. The point density also affects total snow-volume estimation from interpolated raster products. The effect of point density is more significant in densely forested areas than in less-densely forested areas because the under-sampling of data points under canopy and oversampling of data points in the open and drip edge areas can offset the overestimation and underestimation when forest density is moderate. The tree-well snow-depth distribution depends on both topography and the tree above the snow surface, with the statistical analysis over the sampled study plots indicating that more snow accumulated at the down slope direction from the tree bole under each tree, which can be caused by both snow creeping and the thermal radiation emitted by trees. Due to larger interception capacity and stronger thermal radiation from larger trees, the gradient of the tree well increases as the crown area increases. Tree wells with larger gradients are at lower elevations because of larger crown areas. Observed from the 0.5×0.5-m^2 resolution rasters, the snow depth was correlated with tree height, surrounding canopy coverage, tree-height standard deviation, and also crown volume. Both the topographic variables and vegetation variables are important in terms of predicting the snow depth spatially at different scales using the trained XGBoost model.

6. ACKNOWLEDGMENTS

The work presented in this paper is supported by the UC Office of the President's Multi-Campus Research Programs and Initiatives (MR-15-328473) through the UC Water Security and Sustainability Research Initiative (grant no. 13941). We acknowledge the National Science Foundation (NSF) through the Southern Sierra Critical Zone Observatory (NSF Award Numbers 1331939 and 1239521). The data set used in this study can be accessed from the Opentopography web portal (http://opentopo.sdsc.edu/lidarDataset?opentopoID=OTLAS.042013.26911.1, http://opentopo.sdsc.edu/lidarDataset?opentopoID=OTLAS.042013.26911.2).

REFERENCES

1. R. C. Bales, N. P. Molotch, T. H. Painter, M. D. Dettinger, R. Rice, and J. Dozier, "Mountain hydrology of the western United States," Water Resour. Res. **42** (2006).
2. C. Hopkinson, M. Sitar, L. Chasmer, C. Gynan, D. Agro, R. Enter, J. Foster, N. Heels, C. Hoffman, J. Nillson, and Others, "Mapping the spatial distribution of snowpack depth beneath a variable forest canopy using airborne laser altimetry," Proc. 58th Annu. East. Snow Conf. (2001).
3. A. Winstral and D. Marks, "Long-term snow distribution observations in a mountain catchment: Assessing variability, time stability, and the

representativeness of an index site," Water Resour. Res. **50**, 293–305 (2013).
4. D. L. Golding and R. H. Swanson, "Snow distribution patterns in clearings and adjacent forest," Water Resour. Res. **22**, 1931–1940 (1986).
5. R. A. Houze, "Orographic effects on precipitating clouds," Rev. Geophys. **50** (2012).
6. R. Mott, D. Scipión, M. Schneebeli, N. Dawes, A. Berne, and M. Lehning, "Orographic effects on snow deposition patterns in mountainous terrain," J. Geophys. Res. Atmospheres **119**, 1419–1439 (2014).
7. D. Marks, J. Kimball, D. Tingey, and T. Link, "The sensitivity of snowmelt processes to climate conditions and forest cover during rain-on-snow: a case study of the 1996 Pacific Northwest flood," Hydrol. Process. **12**, 1569–1587 (1998).
8. D. Marks, J. Domingo, D. Susong, T. Link, and D. Garen, "A spatially distributed energy balance snowmelt model for application in mountain basins," Hydrol. Process. **13**, 1935–1959 (1999).
9. K. N. Musselman, N. P. Molotch, S. A. Margulis, P. B. Kirchner, and R. C. Bales, "Influence of canopy structure and direct beam solar irradiance on snowmelt rates in a mixed conifer forest," Agric. For. Meteorol. **161**, 46–56 (2012).
10. K. N. Musselman, N. P. Molotch, and P. D. Brooks, "Effects of vegetation on snow accumulation and ablation in a mid-latitude sub-alpine forest," Hydrol. Process. **22**, 2767–2776 (2008).
11. J. E. Sicart, R. L. H. Essery, J. W. Pomeroy, J. Hardy, T. Link, and D. Marks, "A Sensitivity Study of Daytime Net Radiation during Snowmelt to Forest Canopy and Atmospheric Conditions," J. Hydrometeorol. **5**, 774–784 (2004).
12. N. R. Hedstrom and J. W. Pomeroy, "Measurements and modelling of snow interception in the boreal forest," Hydrol. Process. **12**, 1611–1625 (1998).
13. T. R. Roth and A. W. Nolin, "Forest impacts on snow accumulation and ablation across an elevation gradient in a temperate montane environment," Hydrol. Earth Syst. Sci. **21**, 5427–5442 (2017).
14. Z. Zheng, P. B. Kirchner, and R. C. Bales, "Topographic and vegetation effects on snow accumulation in the southern Sierra Nevada: a statistical summary from lidar data," The Cryosphere **10**, 257–269 (2016).
15. R. C. Bales, J. W. Hopmans, A. T. O'Geen, M. Meadows, P. C. Hartsough, P. Kirchner, C. T. Hunsaker, and D. Beaudette, "Soil moisture response to snowmelt and rainfall in a sierra nevada mixed-conifer forest," Vadose Zone J. **10**, 786–799 (2011).
16. R. Rice, R. C. Bales, T. H. Painter, and J. Dozier, "Snow water equivalent along elevation gradients in the merced and tuolumne river basins of the sierra nevada," Water Resour. Res. **47** (2011).
17. A. Varhola, N. C. Coops, M. Weiler, and R. D. Moore, "Forest canopy effects on snow accumulation and ablation: An integrative review of empirical results," J. Hydrol. **392**, 219–233 (2010).
18. M. Jenicek, H. Pevna, and O. Matejka, "Canopy structure and topography effects on snow distribution at a catchment scale: Application of multivariate approaches," J. Hydrol. Hydromechanics **66** (2018).
19. G. Jost, M. Weiler, D. R. Gluns, and Y. Alila, "The influence of forest and topography on snow accumulation and melt at the watershed-scale," J. Hydrol. **347**, 101 – 115 (2007).
20. N. P. Molotch and R. C. Bales, "Scaling snow observations from the point to the grid element: Implications for observation network design," Water Resour. Res. **41**, 1–16 (2005).
21. N. P. Molotch, M. T. Colee, R. C. Bales, and J. Dozier, "Estimating the spatial distribution of snow water equivalent in an alpine basin using binary regression tree models: The impact of digital elevation data and independent variable selection," Hydrol. Process. **19**, 1459–1479 (2005).
22. J. Revuelto, J. I. López-Moreno, C. Azorin-Molina, and S. M. Vicente-Serrano, "Canopy influence on snow depth distribution in a pine stand determined from terrestrial laser data," Water Resour. Res. **51**, 3476–3489 (2015).
23. P. Storck, D. P. Lettenmaier, and S. M. Bolton, "Measurement of snow interception and canopy effects on snow accumulation and melt in a mountainous maritime climate, oregon, united states," Water Resour. Res. **38**, 5–1–5–16 (2002).
24. M. van Heeswijk, J. S. Kimball, and D. Marks, "Simulation of Water Available for Runoff in Clearcut Forest Openings During Rain-On-Snow Events in the Western Cascade Range of Oregon and Washington," Tech. rep., U.S. Geological Survey (1996).
25. J. I. López-Moreno and M. Stähli, "Statistical analysis of the snow cover variability in a subalpine watershed: Assessing the role of topography and forest interactions," J. Hydrol. **348**, 379 – 394 (2008).
26. G. Zheng and L. M. Moskal, "Retrieving Leaf Area Index (LAI) Using Remote Sensing: Theories, Methods and Sensors," Sensors. **9**, 2719–2745 (2009).
27. P. Gowda, T. Oommen, D. Misra, R. Schwartz, T. Howell, and P. Wagle, "Retrieving Leaf Area Index from Remotely Sensed Data Using Advanced Statistical Approaches," J. Remote. Sens. & GIS **05** (2015).
28. J. I. López-Moreno and J. Latron, "Influence of canopy density on snow distribution in a temperate mountain range," Hydrol. Process. **22**, 117–126 (2008).
29. X. Yao, N. Wang, Y. Liu, T. Cheng, Y. Tian, Q. Chen, and Y. Zhu, "Estimation of wheat lai at middle to high levels using unmanned aerial vehicle narrowband multispectral imagery," Remote. Sens. **9** (2017).
30. A. S. Antonarakis, K. S. Richards, J. Brasington, and E. Muller, "Determining leaf area index and leafy tree roughness using terrestrial laser scanning," Water Resour. Res. **46** (2010).
31. M. Kelly and S. Di Tommaso, "Mapping forests with Lidar provides flexible, accurate data with many uses," California Agric. **69**, 14–20 (2015).
32. W. Li, Q. Guo, M. K. Jakubowski, and M. Kelly, "A New Method for Segmenting Individual Trees from the Lidar Point Cloud," Photogramm. Eng. & Remote. Sens. **78**, 75–84 (2012).
33. V. F. Strîmbu and B. M. Strîmbu, "A graph-based segmentation algorithm for tree crown extraction using airborne LiDAR data," ISPRS J. Photogramm. Remote. Sens. **104**, 30–43 (2015).
34. D. Moeser, M. Stähli, and T. Jonas, "Improved snow interception modeling using canopy parameters derived from airborne lidar data," Water Resour. Res. **51**, 5041–5059 (2015).
35. M. L. Goulden, R. G. Anderson, R. C. Bales, A. E. Kelly, M. Meadows, and G. C. Winston, "Evapotranspiration along an elevation gradient in California's Sierra Nevada," J. Geophys. Res. Biogeosciences **117**, n/a–n/a (2012).
36. P. B. Kirchner, R. C. Bales, N. P. Molotch, J. Flanagan, and Q. Guo, "LiDAR measurement of seasonal snow accumulation along an elevation gradient in the southern Sierra Nevada, California," Hydrol. Earth Syst. Sci. Discuss. **11**, 5327–5365 (2014).
37. Z. Zheng, Q. Ma, K. Qian, and R. C. Bales, "Canopy effects on snow accumulation: Observations from lidar, canonical-view photos, and continuous ground measurements from sensor networks," Remote. Sens. **10** (2018).
38. M. Isenburg, "LAStools - efficient LiDAR processing software," (2014).
39. B. Kerkez, S. D. Glaser, R. C. Bales, and M. W. Meadows, "Design and performance of a wireless sensor network for catchment-scale snow and soil moisture measurements," Water Resour. Res. **48** (2012).
40. ESRI, "ArcGIS Desktop," (2015).
41. Q. Guo, W. Li, H. Yu, and O. Alvarez, "Effects of Topographic Variability and Lidar Sampling Density on Several DEM Interpolation Methods," Photogramm. Eng. & Remote. Sens. **76**, 701–712 (2010).
42. J. B. Roerdink and A. Meijster, "The watershed transform: Definitions, algorithms and parallelization strategies," Fundam. Inf. **41**, 187–228 (2000).
43. X. Lin and J. Zhang, "Segmentation-based filtering of airborne lidar point clouds by progressive densification of terrain segments," Remote. Sens. **6**, 1294–1326 (2014).
44. P. F. Felzenszwalb and D. P. Huttenlocher, "Efficient Graph-Based Image Segmentation," Int. J. Comput. Vis. **59**, 167–181 (2004).
45. S. van der Walt, J. L. Schönberger, J. Nunez-Iglesias, F. Boulogne, J. D. Warner, N. Yager, E. Gouillart, and T. Yu, "scikit-image: image processing in Python," PeerJ. **2**, e453 (2014).
46. A. Winstral, K. Elder, and R. E. Davis, "Spatial snow modeling of wind-redistributed snow using terrain-based parameters," J. Hydrometeorol.

3, 524–538 (2002).
47. S. Riley, S. Degloria, and S. Elliot, "A terrain ruggedness index that quantifies topographic heterogeneity," Int. J. Sci. **5**, 23–27 (1999).
48. F. Pedregosa, G. Varoquaux, A. Gramfort, V. Michel, B. Thirion, O. Grisel, M. Blondel, G. Louppe, P. Prettenhofer, R. Weiss, V. Dubourg, J. Vanderplas, A. Passos, D. Cournapeau, M. Brucher, M. Perrot, and É. Duchesnay, "Scikit-learn: Machine Learning in Python," J. Mach. Learn. Res. **12**, 2825–2830 (2011).
49. A. Ohmura, "Physical Basis for the Temperature-Based Melt-Index Method," J. Appl. Meteorol. **40**, 753–761 (2001).
50. R. Rice and R. C. Bales, "An assessment of snowcover in major river basins of sierra nevada network parks and potential approaches for long-term monitoring," Tech. Rep. Natural Resource Technical Report NPS/SIEN/NRTR-2013/800, National Park Service, Fort Collins, Colorado (2013).
51. T. Chen and C. Guestrin, "XGBoost," in *Proceedings of the 22nd ACM SIGKDD International Conference on Knowledge Discovery and Data Mining - KDD '16,* (ACM Press, New York, New York, USA, 2016), pp. 785–794.
52. L. Breiman, "Random forests," Mach. Learn. **45**, 5–32 (2001).
53. J. H. Friedman, "Greedy function approximation: A gradient boosting machine," Annals Stat. **29**, 1189–1232 (2000).
54. J. S. Deems, T. H. Painter, and D. C. Finnegan, "Lidar measurement of snow depth: a review," J. Glaciol. **59**, 467–479 (2013).
55. R. Essery, J. Pomeroy, C. Ellis, and T. Link, "Modelling longwave radiation to snow beneath forest canopies using hemispherical photography or linear regression," Hydrol. Process. **22**, 2788–2800 (2008).
56. R. Howard and R. Stull, "IR Radiation from Trees to a Ski Run: A Case Study," J. Appl. Meteorol. Climatol. **52**, 1525–1539 (2013).
57. H. Lu, W.-s. Wei, M.-z. Liu, X. Han, and W. Hong, "Observations and modeling of incoming longwave radiation to snow beneath forest canopies in the west Tianshan Mountains, China," J. Mountain Sci. **11**, 1138–1153 (2014).
58. C. Webster, N. Rutter, and T. Jonas, "Improving representation of canopy temperatures for modeling subcanopy incoming longwave radiation to the snow surface," J. Geophys. Res. Atmospheres **122**, 9154–9172 (2017).
59. M. Bründl, M. Schneebeli, and H. Flühler, "Routing of canopy drip in the snowpack below a spruce crown," Hydrol. Process. **13**, 49–58 (1999).
60. B. Seyednasrollah and M. Kumar, "Net radiation in a snow-covered discontinuous forest gap for a range of gap sizes and topographic configurations," J. Geophys. Res. **119**, 10,323–10,342 (2014).
61. A. Sumida, T. Miyaura, and H. Torii, "Relationships of tree height and diameter at breast height revisited: analyses of stem growth using 20-year data of an even-aged Chamaecyparis obtusa stand," Tree Physiol. **33**, 106–118 (2013).
62. T. R. Roth and A. W. Nolin, "Characterizing maritime snow canopy interception in forested mountains," Water Resour. Res. **0** (2019).
63. M. Safeeq and C. T. Hunsaker, "Characterizing Runoff and Water Yield for Headwater Catchments in the Southern Sierra Nevada," JAWRA J. Am. Water Resour. Assoc. **52**, 1327–1346 (2016).
64. A. Behrangi, K. J. Bormann, and T. H. Painter, "Using the airborne snow observatory to assess remotely sensed snowfall products in the california sierra nevada," Water Resour. Res. **54**, 7331–7346 (2018).